ECS Transactions, 111 (6) 301-311 (2023)
10.1149/11106.0301ecst ©The Electrochemical Society

Steam Reforming Catalytic Layer on Anode-Supported and Metal-Supported Solid Oxide Fuel Cells for Direct Ethanol Operation

M. Machado[a], F. Tabuti[a], F. Piazzolla[a], T. Moraes[a], R. Abe[b], R. M. Guimarães[b], Y. Miura[c], Y. Fukuyama[c], and F. C. Fonseca[a]

[a] IPEN-CNEN, Nuclear and Energy Research Institute, 05508-000, São Paulo, SP, Brazil
[b] Nissan do Brasil Automóveis Ltda., 04028-900, São Paulo, SP, Brazil
[c] Nissan Motor Co., Ltd., 220-8686, Yokohama, Kanagawa, Japan

A catalyst based on lanthanum chromite with exsolved metallic ruthenium nanoparticles ($LaCrO_3$-Ru) was applied as a catalytic layer for internal ethanol steam reforming of anode-supported and metal-supported solid oxide fuel cells. The metal support exhibits limited catalytic properties for the ethanol steam reforming reaction. Thus, the $LaCrO_3$-Ru catalysts were optimized for operating temperatures in the 600-700 °C range to promote stable ethanol reforming. The catalytic layer had no significant impact on the electrochemical properties of the fuel cell, and samples with and without the catalytic layer exhibited similar performance in hydrogen. Initial durability tests with $LaCrO_3$-Ru layer have shown that the catalytic layer plays a crucial role in the stability of the metal-supported fuel cell under ethanol.

Introduction

Alternative solid oxide fuel cell (SOFC) designs using passive supports have been introduced to exceed the limits of supported cells in ceramic components. The most interesting prospect is to use a metallic material as the cell's support due to its lower cost, greater mechanical strength, and fast start-up. (1–3). These improved properties of the SOFC allow for its use in applications previously reserved for polymeric fuel cells, such as in transportation (4–6). Additionally, due to the high operating temperature of an SOFC (>600 °C), alternative fuels, such as ethanol, already supplied to combustion engine vehicles, can also be supplied to the cell.

Nonetheless, when ethanol is directly fed into the cell, deposits of carbon will form on the surface of the exposed layer leading to a fast and irreversible deactivation of the fuel cell (7). Thus, strategies have been proposed to minimize carbon deposition in the cell. An approach is to use a functional layer with an optimized catalyst for the ethanol steam reforming (ESR) reaction (Eq. 1) (8,9). In previous works, Ir/CGO catalysts were developed and applied successfully as a catalytic layer on anode-supported SOFC operating with anhydrous ethanol. The cell exhibited a stable performance under the operation conditions (10). Iridium, however, is not readily available and is regarded as a noble metal, hence the necessity to develop efficient catalysts viable for a scaled-up production for application in SOFC. And as with the anode-supported cell design, the metal-supported cell (MS-SOFC) also requires the addition of a catalytic layer to reform the fuel (11).

$$CH_3CH_2OH + 3H_2O \leftrightharpoons 6H_2+2CO_2 \quad [1]$$

Attractive materials that can be used as catalysts are perovskites. The ABO_3 structure allows for doping in the A and B-site to fine-tune the electronic, magnetic, and catalytic properties of the compound. Lanthanum chromite ($LaCrO_3$) is a perovskite that exhibits high stability at a wide range of temperatures and pressures and has a resistance to grain coarsening (12,13), favorable characteristic for a catalyst support. Doping the B-site of lanthanum chromite with Ru has been shown to enhance the catalytic property of the perovskite for hydrogen production (14–18). By the exsolution of the active metal, the catalytic activity of the oxide material can further be promoted. The exsolution process guarantees a homogeneous distribution of metallic nanoparticles and a strong interaction between the ceramic matrix and the active metal (19,20).

In this present study, lanthanum chromite with exsolved metallic ruthenium nanoparticles ($LaCrO_3$-Ru) was evaluated as a catalytic material for ethanol steam reforming reaction at 600 °C. The suitability of the application of catalytic layers on SOFC was established. Hence, the $LaCrO_3$-Ru catalyst was applied as a catalytic layer on a MS-SOFC and the stability of the cell at 700 °C under anhydrous ethanol was assessed.

Experimental

Synthesis and Characterization of Catalyst

The Pechini method was used to synthesize the ceramic powders of $La(Cr_{1-x}Ru_x)O_{3-\delta}$, where x = 0 and 0.20 (21,22). Accordingly, an aqueous solution of $La(NO_3)_3.6H_2O$ (99.9% Sigma Aldrich), $Cr(NO_3)_3.9H_2O$ (99.9%, Sigma Aldrich), and $RuCl_3.nH_2O$ (99.9%, Sigma Aldrich) was mixed with citric acid for 2 h. Ethylene Glycol was added to the solution and heated to 180 °C until the production of an organic resin. The resin was calcined in air at 1000 °C for 1 h. For the synthesis, the molar ratio of 1:2:4 of metallic cations: citric acid: ethylene glycol was used. The exsolution of Ru was carried out by a heat treatment in reducing atmosphere of the calcined powders (23). The utilized conditions were: 900 °C for 4 h in H_2 (99.999%).

X-ray diffraction analyses of the calcined powders of $LaCrO_3$ (LCO) and $La(Cr_{0.8}Ru_{0.2})O_{3-\delta}$ with Ru exsolved (LCRu) were performed using a Miniflex II model diffractometer with Cu-Kα radiation source (0.15406 nm) in the range of 20° to 90° 2θ. Scanning electron microscopy (SEM) and transmission electron microscopy (TEM) analyses of the ceramic powder with the exsolved Ru were carried out using the JEOL microscope (model JMS-6701F) equipped with a field emission gun (FEG-SEM) and the TEM images were collected by the JEOL microscope (model JEM-2010)

The ethanol steam reforming (ESR) reactions of the ceramic powders and of the metallic support of the SOFC (composed mainly of Fe and Cr) were performed in a fixed bed quartz tubular reactor packed with 50 mg in a vertical oven at a temperature of 600 °C for the ceramic powders and at 700 °C for the metallic support. Water and ethanol were fed into the reactor using a system with two saturators to obtain a H_2O/CH_3CH_2OH molar ratio of 3. The ethanol conversion ($X_{ethanol}$) and selectivity (S_{xl}) of the obtained products as

a function of the reaction time were determined by (Eqs. 2 and 3). The reactants and the reaction products were analyzed by gas chromatography (Agilent 7890A), equipped with a thermal conductivity detector (TCD) and a flame ionization detector (FID) connected in series.

$$X_{ethanol} = ((n_{ethanol})_{fed} - (n_{ethanol})_{exit})) / (n_{ethanol})_{fed} * 100 \quad [2]$$

$$S_{xl} = (n_x)_{produced}/(n_{totall})_{produced}) * 100 \quad [3]$$

Catalytic Layer Deposition and Fuel Cell Testing

An initial electrochemical test to investigate the viability of the application of a catalytic layer was carried out on an anode supported cell (Fuel Cell Materials). The catalyst used for the layer was one previously reported by the group, Ir/CGO (10). The fuel cell was mounted on the test set-up from Fiaxell SOFC Technologies™, with Au current collectors in the air outlet and on the fuel side. The electrochemical workstation Zahner IM6 was used to collect data from the cell.

A MS-SOFC with catalytic layer (CL-MS-SOFC) was prepared for a durability assessment. Prior to the deposition of the catalytic layer, Au was painted on the anode and a gold wire was fixed for current collection, as shown in Figure 1a. The catalytic ink based on the LCRu20 ceramic powder was fabricated by ball milling the catalytic powder with terpineol and isopropanol, followed by its deposition on the metal support of MS-SOFC by the airbrush technique. To eliminate the organics of the ink and for the attachment of the catalytic layer on the metal support the cell was pre-treated at 200 °C in air and then sintered at 800 °C for 5 h under H_2. The fuel cell after the heat treatment is shown in Figure 1b. The effectiveness of the mentioned heat treatment was evaluated by the morphology assessment of the catalytic layer deposited on a YSZ substrate using the JEOL SEM model JSM-6010LA.

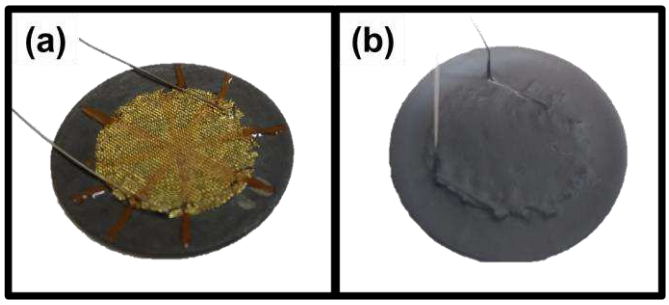

Figure 1. (a) Image of the MS-SOFC with a gold paste and a gold wire current collection and (b) image of the cell with the deposition of the catalytic layer (CL-MS-SOFC).

The durability test under anhydrous ethanol of the MS-SOFC (as-received) and of the CL-MS-SOFC were carried in a test set-up from Fiaxell SOFC Technologies™ and the data was obtained though the workstation Zahner IM6. The cells operated under a polarization of 0.6 V at 700 °C, first with H_2 and then the fuel was changed to ethanol. A

stoichiometric ratio of ethanol to hydrogen of 1:6 was used for the durability test, giving a gas composition of 42% H_2 in N_2 and 7% ethanol diluted in N_2.

Results and Discussion

Characterization and Performance of Catalyst

Figure 2 shows the highly crystalline XRD patterns of LCO, after calcination and LCRu, after reduction (exsolution of Ru). The samples correspond to the standard characteristic peaks of the Pbnm symmetry compatible with the lanthanum chromite (ICSD#9938) (24). The pattern of the LCRu sample did not show detectable peaks related to the formation of exsolved metallic Ru. It is, nonetheless, expected that the formation of exsolved Ru^0 species is lower than the nominal value of the dopant (x = 0.2), such that it can be difficult to detect in an XRD analysis (25).

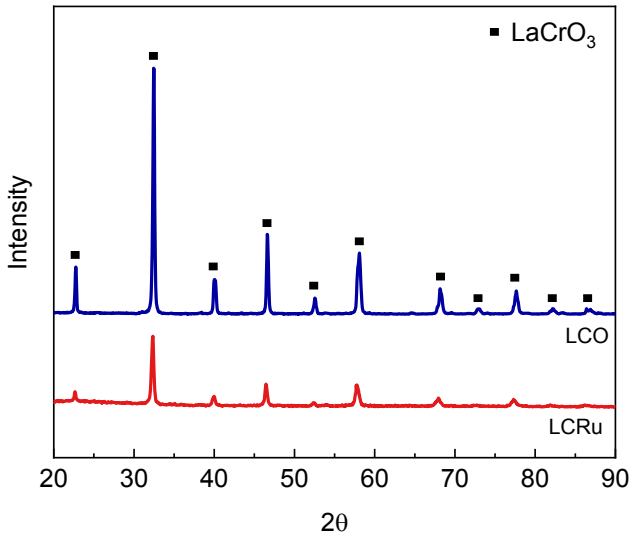

Figure 2. XRD patterns of LCO (after calcination) and LCRu (after exsolution of Ru).

The morphology of the LCRu20 was examined by scanning electron microscopy (SEM) and transmission electron microscopy (TEM) as presented in Figure 3a and b, respectively. The SEM image shows grains with an average dimension of 100 nm. It is visible on the SEM image of the ceramic powder a start of the sintering process i.e., neck formation, which is due to the high temperatures applied for calcination (1000 °C) and reduction (900 °C). The exsolved Ru nanoparticles are not distinguishable in the SEM image but are revealed in the TEM image. In the TEM image, nanometric protrusions with spherical sizes of around 5 nm are observed on the surface of the LCRu particles. The protrusions appear to be socked on the substrate, consistent with nanoparticles formed by the exsolution process as previously reported (25,26).

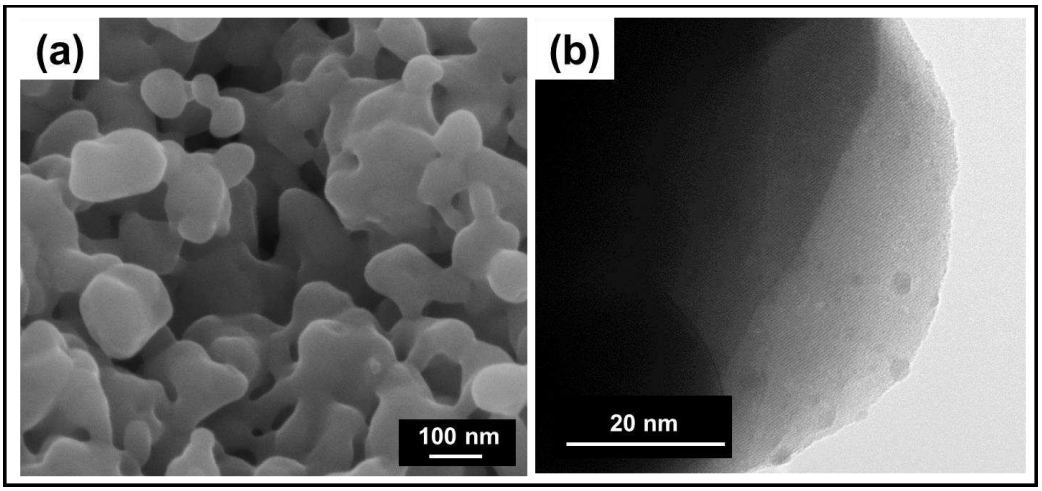

Figure 3. (a) Scanning electron microscopy and (b) transmission electron microscopy images of LCRu.

The ceramic samples LCO and LCRu, as well as the metallic substrate of the MS-SOFC, were studied for ethanol steam reforming (ESR). The graphs exhibiting the ethanol conversion and product selectivity as a function of time on stream for the ethanol steam reforming reactions at 600 °C on the ceramic powders are shown in Figures 4a and b. The LCO sample, Figure 4a, exhibits poor catalytic performance, with very slight activity for the ESR reaction, where the main product formed (~90%) is acetaldehyde (CH_3CHO) and only ~5% H_2 is formed. The main reaction taking place at 600 °C with LCO as a catalytic material is the dehydrogenation of ethanol into acetaldehyde, as shown in Eq. 4. On the other hand, the LCRu sample exhibits excellent ESR performance (Figure 4b). When Ru is added to the synthesis of LCO, and the perovskite is further reduced to drive the exsolution of Ru^0 nanoparticles, then the catalyst becomes active for H_2 production. Through the 20 h time on stream at 600 °C there is a 100% ethanol conversion and a ~70% selectivity towards the production of H_2. The results emphasize that doping LCO on the B-site with Ru changes the catalytic behavior of the material to an active catalyst with excellent activity for the ESR reaction. Hence, LCRu20 is a viable catalyst for application as a catalytic layer for internal ethanol steam reforming of a MS-SOFC.

The active role of the metal support of a MS-SOFC towards the ESR reaction at 700 °C was assessed. The ethanol conversion and product selectivity as a function of time on stream for the ethanol steam reforming reaction at 700 °C are shown in Figure 4c. Similar to LCO a high activity is observed for the dehydrogenation of ethanol into acetaldehyde (Eq. 4), equivalent to a selectivity of ~70% towards acetaldehyde and of < 20% towards H_2. The extremely limited catalytic properties of the metallic support for the ethanol steam reforming reaction reinforces the difficulty of such cells to operate without a catalytic layer.

$$C_2H_5OH \rightleftharpoons CH_3CHO + H_2 \quad [4]$$

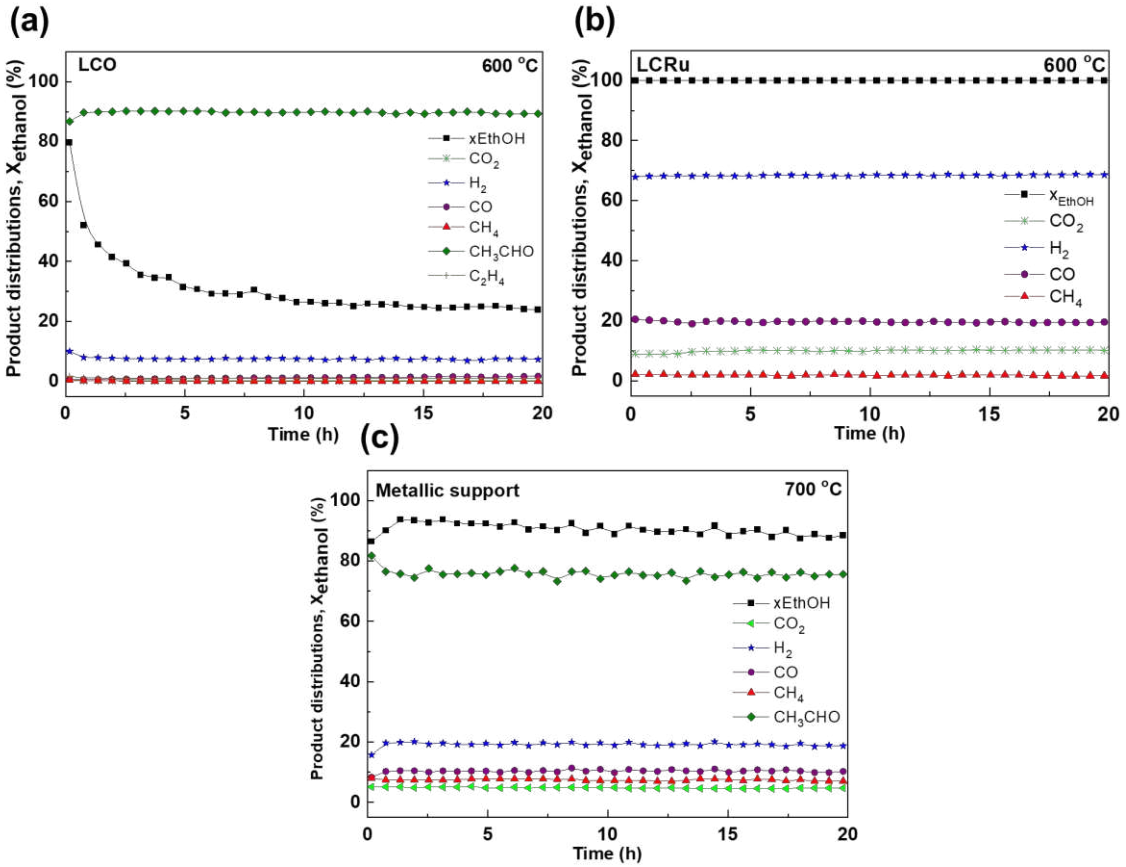

Figure 4. Ethanol conversion and product distribution obtained for the samples during ethanol steam reforming reactions, H_2O/ethanol molar ratio of 3, for (a) LCO at 600 °C, (b) LCRu at 600 °C, and (c) metallic support at 700 °C.

Fuel Cell Testing

The experimental results showed that the LCRu exhibited a high catalytic activity at 600 °C towards ethanol steam reforming, thus a viable option for application as a catalytic layer in for an SOFC operating directly with ethanol. The electrochemical performance of an anode-supported cell with and without catalytic layer was evaluated to ensure that the application of the catalytic layer, subsequent heat treatment and the methodology used for the current collection were efficient. The catalyst used for the layer was one previously reported by the group (10). The *j*-V and *j*-P characteristics of the cell with and without catalytic layers are shown in Figure 5.

Both cells exhibited OCV ~1.1 V and similar *j*-V/ *j*-P characteristics at 700 °C under H_2. At 0.7 V the cell without the catalytic layer displayed a current density of 1.3 $A \cdot cm^{-2}$ and the one with a catalytic layer had a current density of 1.6 $A \cdot cm^{-2}$. Indeed, the sample with the catalytic layer showed better performance, however, differences can be attributed to variations in properties between samples and small differences in the current collection. Nonetheless, the result to be emphasized is that the catalytic layer does not interfere with the electrochemical properties of the fuel cell under the tested conditions, such that cells with and without the catalytic layer exhibit similar performance in hydrogen.

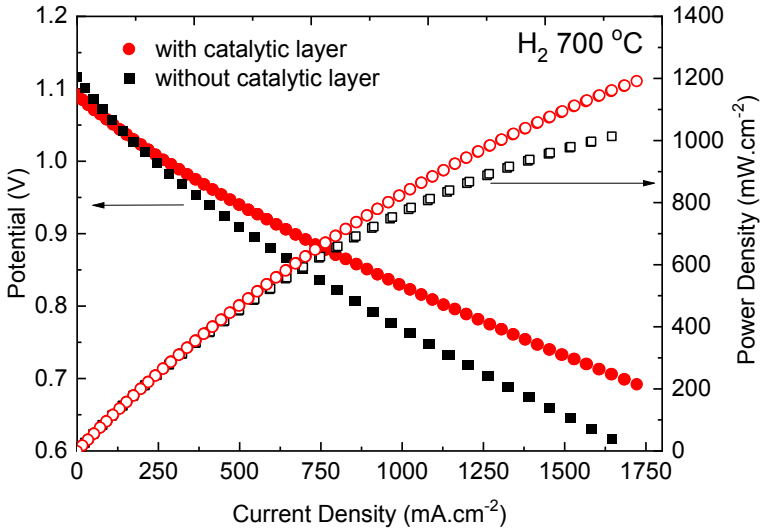

Figure 5. *j*-V and *j*-P characteristics of the anode-supported cell with and without a catalytic layer at 700 °C under H_2.

Prior to the deposition on the MS-SOFC, the catalytic layer was deposited on YSZ, and heat treated. The microstructural features of the layer were evaluated by SEM (Figure 6). The catalytic layer shows a desirable porous structure with a thickness of ~110 µm. In the inset image, it is possible to observe open porosity and well-distributed pores. Such features were achieved without the use of pore formers and highlight that the used method was successful in fabricating a porous catalytic layer.

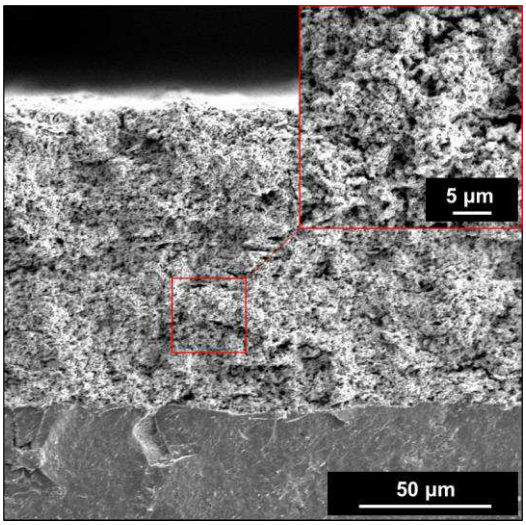

Figure 6. SEM image of the cross-section of the LCRu catalytic layer deposited on a YSZ substrate and inset image of a magnified section of the catalytic layer.

To investigate the effect of the catalytic layer on the electrochemical performance of the MS-SOFC directly fed with anhydrous ethanol, durability tests were carried out of the cell with catalytic layer (CL-MS-SOFC) and without the catalytic layer (MS-SOFC) at 700 °C under 0.6 V polarization (Figure 7a and b). The test was run under the flow of synthetic air on the cathode side, and for the first 11 h, H_2 was used as a fuel and then was changed to ethanol. The flow rates were calculated to carry an equivalent theoretical number of electrons to the anode.

Both cells started at 0.6 V with a current density close to 2 $A \cdot cm^{-2}$, the MS-SOFC with 2.1 $A \cdot cm^{-2}$ and the CL-MS-SOFC with 1.9 $A \cdot cm^{-2}$. The slight difference in performance may be attributed to differences in the current collection, as previously mentioned. The degradation rates for the first 11 h under H_2 were also similar; −24.1 $mA \cdot h^{-1}$ and −22.7 $mA \cdot h^{-1}$ for the MS-SOFC and the CL-MS-SOFC, respectively. By changing the fuel to ethanol there was a drop in the current output. The current output after ~10 min of the MS-SOFC under anhydrous ethanol reached 0. For the CL-MS-SOFC there were significant changes in the current density in the first 2 h under ethanol, from 1.7 $A \cdot cm^{-2}$ to 0.45 $A \cdot cm^{-2}$. Several aspects can be considered as potential reasons for such a drop in current. Parameters such as residence time, difference in mass transport of the fuel, limited H_2 conversion as well as deactivation of the catalyst can contribute to the decrease in efficiency of the cell under ethanol. Nevertheless, after the sudden current drop, there is a rather slower degradation of the fuel cell under ethanol, accounting for ~12.2 $mA \cdot h^{-1}$, reaching a current density of 94.4 $mA \cdot cm^{-2}$ after 42 h of operation. The preliminary results of the durability test of the MS-SOFC have emphasized the requirement of a catalytic layer for cells operating directly under ethanol and that advances are needed to minimize the loss in efficiency associated with the current drop when the fuel is changed from H_2 to ethanol.

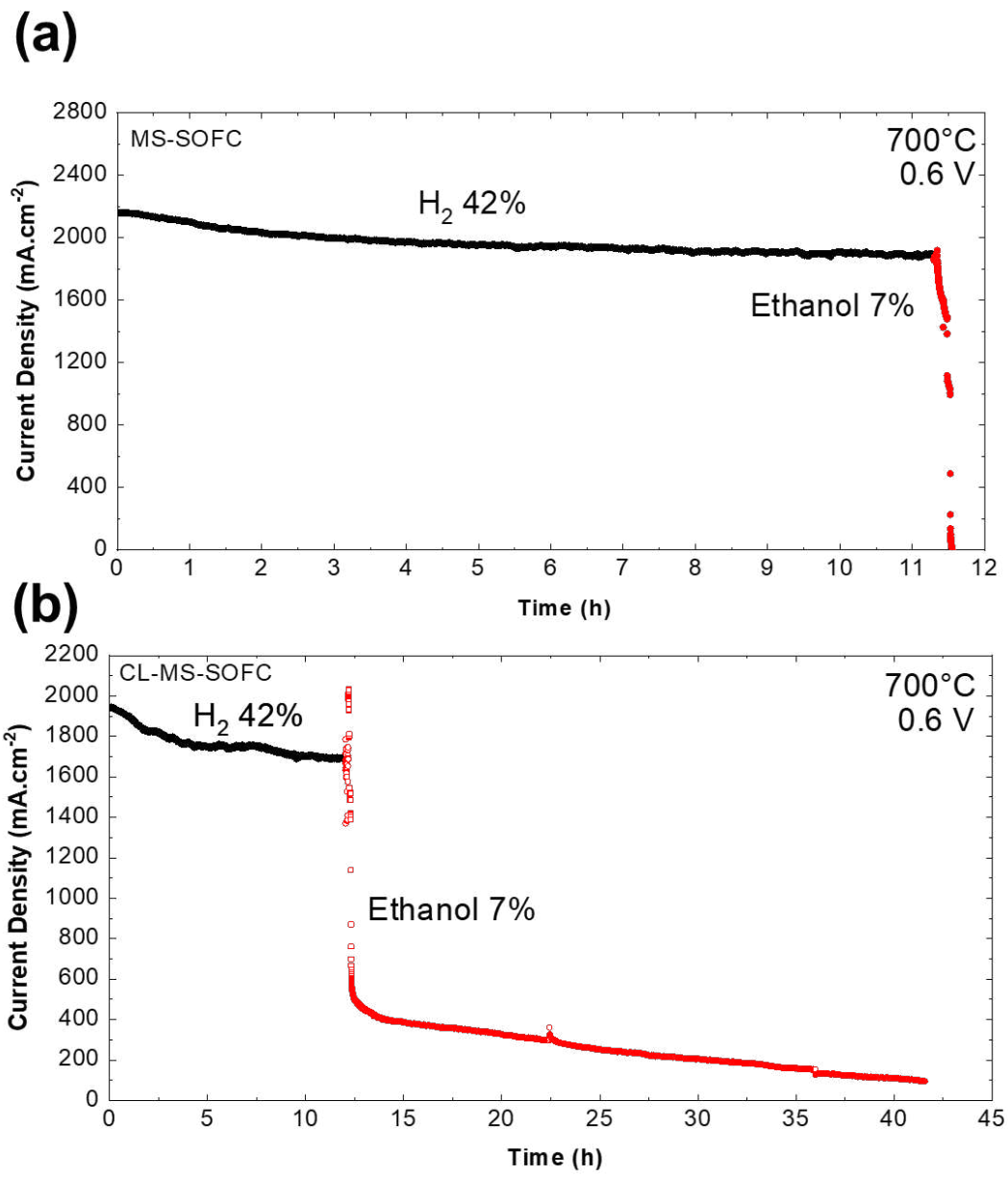

Figure 7. Durability test of the metal-supported single cells at 700 °C and applied voltage of 0.6 V under H_2 and anhydrous ethanol: (a) without a catalytic layer (MS-SOFC) and (b) with a LCRu catalytic layer (CL-MS-SOFC).

Conclusion

A lanthanum chromite with exsolved ruthenium nanoparticles with excellent catalytic activity for ethanol steam reforming was successfully synthesized. Such catalyst was used as a catalytic layer for internal ethanol steam reforming on solid oxide fuel cells. The applied catalytic layer on an anode-supported fuel cell was shown to not interfere with the electrochemical properties of the fuel cell operating with hydrogen. The metallic support promotes ethanol dehydrogenation resulting in acetaldehyde production and low selectivity to hydrogen. Thus, metal-supported SOFC running on ethanol shows a steep drop in current and fast fuel cell deactivation. In contrast, the fuel cell with the $LaCrO_3$-Ru catalytic layer

exhibits improved stability under direct operation with anhydrous ethanol at 700 °C. The preliminary result demonstrates the $LaCrO_3$-Ru catalytic layer was effective in reforming ethanol into hydrogen and hence improves the performance of a MS-SOFC under ethanol.

Acknowledgments

Authors would like to acknowledge the support from Nissan and the Brazilian agencies FAPESP grants n° 2019/15110-2 and 2022/06295-1, and CNPq Sis-H_2 grant n° 407967/2022-2. FCF is CNPq fellow.

References

1. M. C. Tucker, *J. Power Sources*, **195**(15), 4570–4582 (2010).
2. Q.-A. Huang, J. Oberste-Berghaus, D. Yang, S. Yick, Z. Wang, B. Wang, and R. Hui, *J. Power Sources*, **177**(2), 339–347 (2008).
3. M. C. Tucker, G. Y. Lau, C. P. Jacobson, L. C. DeJonghe, and S. J. Visco, *J. Power Sources*, **175**(1), 447–451 (2008).
4. E. Dogdibegovic, Y. Fukuyama, and M. C. Tucker, *J. Power Sources*, **449**, 227598 (2020).
5. A. Hagen, X. Sun, B. R. Sudireddy, and Å. H. Persson, *J. Electrochem. Soc.* **167**(10), 104510 (2020).
6. M. Dewa, W. Yu, N. Dale, A. M. Hussain, M. G. Norton, and S. Ha, *Int. J. Hydrog. Energy*, **46**(67), 33523–33540 (2021).
7. N. Laosiripojana and S. Assabumrungrat, *J. Power Sources*, **163**(2), 943–951 (2007).
8. S. D. Nobrega, M. V. Galesco, K. Girona, D. Z. de Florio, M. C. Steil, S. Georges, and F. C. Fonseca, *J. Power Sources*, **213**, 156–159 (2012).
9. N. K. Monteiro, F. B. Noronha, L. O. O. da Costa, M. Linardi, and F. C. Fonseca, *Int. J. Hydrog. Energy*, **37**(12), 9816–9829 (2012).
10. M. C. Steil, S. D. Nobrega, S. Georges, P. Gelin, S. Uhlenbruck, and F. C. Fonseca, *Appl. Energy*, **199**, 180–186 (2017).
11. M. Dewa, M. A. Elharati, A. M. Hussain, Y. Miura, D. Song, Y. Fukuyama, Y. Furuya, N. Dale, X. Zhang, O.G. Marin-Flores, D. Wu, M.G. Norton, and S. Ha, *J. Power Sources*, **541**, 231625 (2022).
12. S. Gupta, M. K. Mahapatra, and P. Singh, *Mater. Res. Bull.*, **48**(9), 3262–3267 (2013).
13. N. Sakai, T. Kawada, H. Yokokawa, M. Dokiya, and T. Iwata, *J. Mater. Sci.*, **25**(10), 4531–4534 (1990).
14. S. Georges, G. Parrour, M. Henault, and J. Fouletier, *Solid State Ion.,* **177**(19–25), 2109–2112 (2006).
15. P. Vernoux, E. Djurado, and M. Guillodo, *J. Am. Ceram. Soc.*, **84**(10), 2289–2295 (2004).
16. P. Vernoux, J. Guindet, and M. Kleitz, *J. Electrochem. Soc.*, **145**(10), 3487–3492 (1998).
17. N. Mota, I. Z. Ismagilov, E. V. Matus, V. V. Kuznetsov, M. A. Kerzhentsev, Z. R. Ismagilov, R. M. Navarro, and J. L. G. Fierro, *Int. J. Hydrog. Energy*, **41**(42), 19373–19381 (2016).
18. Y. Jeon, O. Kwon, C. Lee, G. Lee, J. Myung, S. Sun Park, J. T. S. Irvine, and Y. Shul, *Appl. Catal. A*, **582**, 117111 (2019).

19. A. C. W. Koh, W. K. Leong, L. Chen, T. P. Ang, J. Lin, B. F. G. Johnson, and T. Khimyak, *Catal. Commun.*, **9**(1), 170–175 (2008).
20. A. C. W. Koh, L. Chen, W. K. Leong, T. P. Ang, B. F. G. Johnson, T. Khimyak, and J. Lin, *Int. J. Hydrog. Energy*, **34**(14), 5691–5703 (2009).
21. M. P. Pechini, Method of preparing lead and alkaline earth titanates and niobates and coating method using the same to form a capacitor, *United States Patent Office*, 01–07 (1967).
22. D. Segal, *J. Mater. Chem.*, **7**(8), 1297–1305 (1997).
23. K. Kousi, C. Tang, I. S. Metcalfe, and D. Neagu, *Small*, **17**(21), 2006479 (2021).
24. M. Hellenbrandt, *Crystallography Reviews*, **10**(1), 17–22 (2004).
25. V. B. Tinti, D. Marani, A. S. Ferlauto, F. C. Fonseca, V. Esposito, and D. Z. Florio, *Part. Part. Syst. Charact.*, **37**(2), 1900472 (2020).
26. D. Neagu, T.-S. Oh, D. N. Miller, H. Ménard, S. M. Bukhari, S. R. Gamble, R. J. Gorte, J. M. Vohs, and J. T. S. Irvine, *Nat. Commun.*, **6**(1), 8120 (2015).